

Supplement of Atmos. Chem. Phys., 16, 11237–11248, 2016
<http://www.atmos-chem-phys.net/16/11237/2016/>
doi:10.5194/acp-16-11237-2016-supplement
© Author(s) 2016. CC Attribution 3.0 License.



Atmospheric
Chemistry
and Physics
Open Access
EGU

Supplement of

Impact of NO_x and OH on secondary organic aerosol formation from β-pinene photooxidation

Mehrnaz Sarrafzadeh et al.

Correspondence to: Jürgen Wildt (j.wildt@fz-juelich.de)

The copyright of individual parts of the supplement might differ from the CC-BY 3.0 licence.

1 In this supplement we describe how wall losses of low volatile compounds were determined
2 and how the measured masses were corrected for these wall losses (Sects. S1 and S2). In
3 addition, it is described how yields were obtained from steady state conditions (Sect. S3). In
4 Sect. S4 we estimate possible errors of the correction procedure and give information on the
5 error bars given in the manuscript.

6

7 **S1 Consideration of wall losses of HOMs for determinations of particle mass formation**

8 Mass yields determined in different chambers and under different condition may vary
9 substantially because there is an operational component in SOA-yield determinations. In
10 particular wall losses of vapours and particles have impacts on the results. We therefore
11 carefully studied wall losses of particles as well as their important precursors. We also studied
12 losses of vapours on seed particles and compared the loss rates on walls to loss rates on
13 particles. With the knowledge of these losses we developed a method allowing correcting
14 mass yields for wall losses of important precursors.

15 Important precursors of particles in our chamber are extreme low volatile organic compounds,
16 ELVOCs (Ehn et al., 2014), a subgroup of the highly oxidized multifunctional compounds
17 termed as HOMs (Mentel et al., 2015). HOMs are products of ozonolysis (Mentel et al., 2015)
18 and photooxidation. They contain many O atoms and they are measurable in the gas phase by
19 a Chemical Ionisation time of flight Mass Spectrometer using NO_3^- reagent ions (NO_3^- –
20 *CIMS*).

21 With the NO_3^- – *CIMS* the elemental composition of HOMs (C, H, O and if abundant N
22 atoms) can be determined, whereas chemical properties and functionalization of the HOMs
23 cannot. However, the physical properties investigated here are independent of the chemical
24 behaviour of the HOMs; we studied their losses on particles and chamber walls.

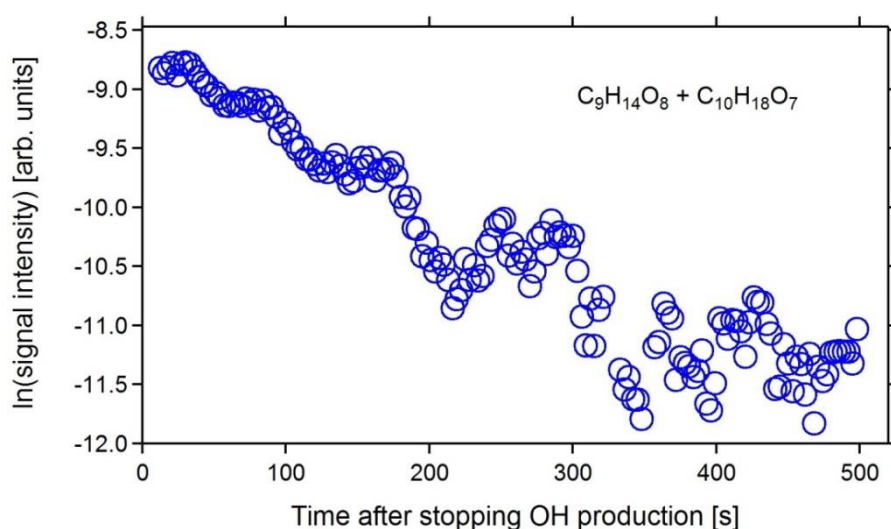
25 HOMs were produced from OH initiated oxidation of α -pinene and β -pinene. As general
26 result, the behaviour of HOMs with respect to wall losses and losses on particles was very
27 similar for α -pinene and β -pinene. Although examples shown below are from either of
28 BVOCs they also represent results for the other BVOC.

29 Losses of HOMs on the walls of our continuously stirred tank reactor were measured as
30 described by Ehn et al. (2014). Briefly, the chamber was flushed with the respective BVOC at
31 concentrations below 1 ppb. The low concentrations were chosen to keep particle formation
32 as low as possible ensuring that the chamber walls are the dominant condensational sink.

1 HOMs were produced from photooxidation and, when signal intensities were in steady state,
2 the UV lamp used for OH production was switched off. This led to a fast decay of signal
3 intensity for most of the HOMs.

4 At VOC concentrations around 1 ppb, the lifetime of OH is less than a second. The decay
5 observed for the signal intensities of different HOMs therefore could directly be used to
6 determine the loss rates of HOMs or their lifetimes, respectively. Logarithms of the values
7 obtained for the signal intensities of given HOMs were plotted versus time and loss rates were
8 obtained from linear regression analysis (see Fig. S1).

9



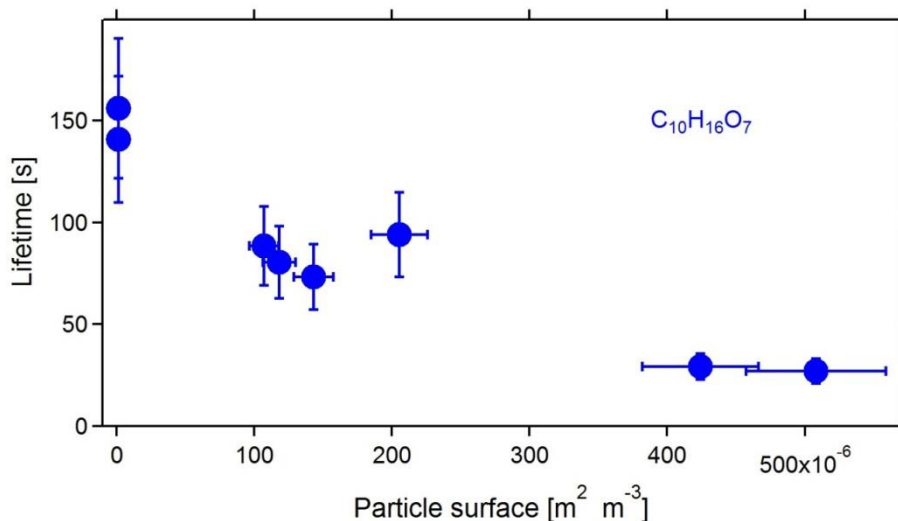
10

11 **Figure S1.** Logarithm of signal intensities for the sum of two HOMs produced from β -pinene
12 photooxidation versus time. Time resolution for individual data points was 3 s and the data
13 were smoothed by a 3-point running average. β -pinene HOM spectra often showed 2 peaks at
14 a given mass that were not fully resolved. Intensities of such peaks were taken as sum. From
15 linear regression analysis of the example shown in Fig. S1, a lifetime of ~ 170 s was obtained
16 (loss rate $0.0058 \pm 0.0002 \text{ s}^{-1}$). Although errors from linear regression analysis were often
17 quite low, we estimate the error for the lifetimes to $\pm 20\%$ since the background was often
18 not easily assessable (residual HOMs from ozonolysis in particular for α -pinene).

19

20 All results obtained with respect to wall losses were similar to the results given by Ehn et al.
21 (2014). The lifetime of the dominant HOMs produced from α -pinene and β -pinene in absence
22 of particles was in the range of 2 to 3 minutes (see supplementary material to Ehn et al.,
23 2014).

- 1 We furthermore observed that the lifetime of HOMs depended on the presence of particles.
- 2 The higher the particle condensational sink, the shorter was the lifetime (Fig. S2).



3
 4 **Figure S2.** Lifetimes determined from linear regression analysis of HOM signal intensities
 5 (see Fig. S1) plotted versus the particle surface. Example is a HOM produced from α -pinene
 6 photooxidation ($\text{C}_{10}\text{H}_{16}\text{O}_7$). Measurements were made for different amounts of particles that
 7 were produced during photooxidation at different α -pinene concentrations. Errors of lifetimes
 8 were estimated to $\pm 20\%$.

9
 10 Time resolved measurements of lifetimes required time resolution for HOM measurements
 11 below 10 s. For many HOMs the signals were too noisy to allow reliable determinations of
 12 decay rates at such time resolution. We therefore used measurements at steady state
 13 conditions allowing integrating HOM signals over several minutes.

14 During such measurements production rates of HOMs were kept constant by keeping the
 15 concentrations of the BVOC, O_3 and OH constant. Seed particles were added and removed
 16 from the chamber. Lifetimes of HOMs or the respective loss rates were determined as
 17 follows:

18 The concentration of a given HOM, $c(\text{H})$, is determined by its production rate $P(\text{H})$ divided by
 19 its first order loss rate $L(\text{H})$ (or multiplied by its lifetime $\tau(\text{H})$, Eq. ES1):

$$c(\text{H}) = \frac{P(\text{H})}{L(\text{H})} = P(\text{H}) \cdot \tau(\text{H}) \quad (\text{ES1})$$

1 Assuming that the signal intensity is proportional to the concentration of the HOM allows
 2 exchanging $c(H)$ by $S(H) \cdot \alpha$, where $S(H)$ is the signal intensity measured for the given HOM
 3 and α is a constant replacing the so far unknown calibration of the $NO_3^- - CIMS$.

4 Due to the efficient losses on the chamber walls and on particles, $\tau(H)$ was often below 2
 5 minutes. The residence time of the air in the chamber was ~ 45 minutes; hence, the outflow of
 6 HOMs out of the chamber was negligible compared to the dominant losses. For chemically
 7 unreactive (closed shell) HOMs these are wall losses, $L_W(H)$, and losses on particles, $L_P(H)$.
 8 For constant production rate $P(H)$ it follows:

$$S(H) \cdot \alpha = \frac{P(H)}{L_W(H) + L_P(H)} = P(H) \cdot \tau(H) \quad (ES2)$$

9 Forming the ratio of signal intensities measured for a given HOM at negligible particle
 10 surface (indexed by “0”) over the signal intensity obtained in measurements with particle
 11 surface, respectively directly reflects the ratio of the lifetimes. The unknown calibration
 12 factors as well as the constant production rates cancel out:

$$\frac{S(H)^0}{S(H)} = \frac{\tau(H)^0}{\tau(H)} = \frac{L_W(H) + L_P(H)}{L_W(H)} \quad (ES3)$$

13 The loss rates of HOMs on particles, $L_P(H)$, can therefore be determined from Eq. (ES4):

$$L_P(H) = \frac{S(H)^0}{S(H)} \cdot L_W(H) - L_W(H) \quad (ES4)$$

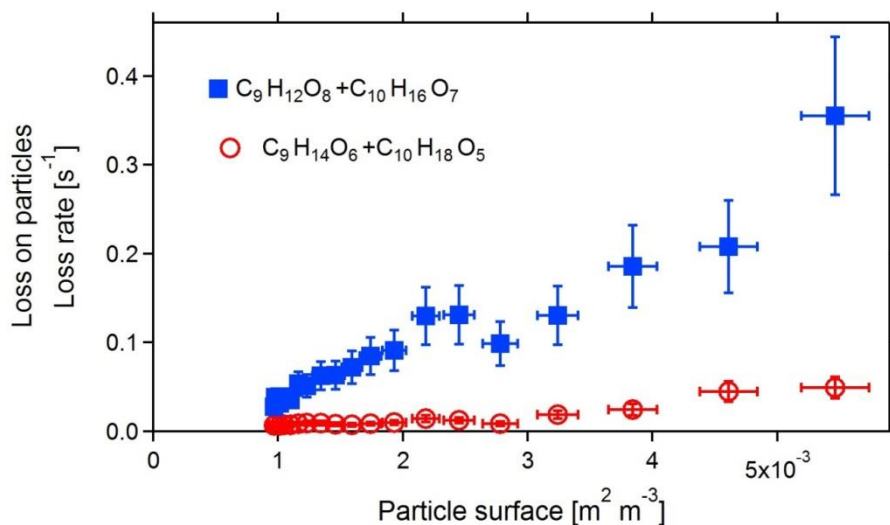
14 Based on kinetic gas theory, L_P can be set to:

$$L_P(H) = \gamma_{eff} \cdot \frac{\bar{v}}{4} \cdot S_P \quad (ES5)$$

15 where \bar{v} is the mean velocity of the HOM, S_P is the surface of the particles during the
 16 respective measurement, and γ_{eff} is an effective uptake coefficient.

17 According to Eq. (ES5), $L_P(H)$ linearly depends on the existing particle surface. The
 18 measured linear relationship between $L_P(H)$ as determined according to Eq. (S4) and the
 19 measured particle surface (Fig. S3) is therefore understandable.

1



2

3 **Figure S3.** Loss rates of β -pinene HOMs in dependence of particle surface. Production rates
 4 of HOMs were constant ($[\beta\text{-pinene}] = 12.8 \text{ ppb}$, $[\text{OH}] = (7.2 \pm 0.6) \times 10^7 \text{ cm}^{-3}$). Particle
 5 surface was varied by varying ammonium sulfate particle concentrations (0 to $\sim 88.5 \mu\text{g}$ using
 6 a density of 1.77). For β -pinene the HOM spectra often showed 2 peaks at integer masses that
 7 were not fully resolved. Such peaks were plotted as sum. In particular at high particle surface
 8 the signal intensities may be very low and errors for the signal intensities may be high. Errors
 9 were estimated to $\pm 25 \%$.

10

11 Dividing the slopes of plots such as shown in Fig. S3 (slope = $\gamma_{eff} \cdot \frac{\bar{v}}{4}$) by $\frac{4}{\bar{v}}$ leads to the
 12 effective uptake coefficient γ_{eff} . For the examples shown in Fig. S3, this procedure led to
 13 $\gamma_{eff} = 1.1 \pm 0.25$ for the sum of $\text{C}_9\text{H}_{12}\text{O}_8 + \text{C}_{10}\text{H}_{16}\text{O}_7$ and to $\gamma_{eff} = 0.15 \pm 0.038$ for $\text{C}_9\text{H}_{14}\text{O}_6$
 14 $+ \text{C}_{10}\text{H}_{18}\text{O}_5$.

15 For most of the HOMs we obtained linear relationships allowing determining effective uptake
 16 coefficients. For HOMs with odd masses we did not interpret the data in this way because we
 17 assumed that these HOMs are radicals. Besides losses on walls and on particles there are
 18 reactive losses which may cause a complicated behaviour of signal intensities. However, these
 19 radicals were only a minor fraction of the HOMs and they were neglected for further
 20 considerations regarding losses on particles and formation of particle mass.

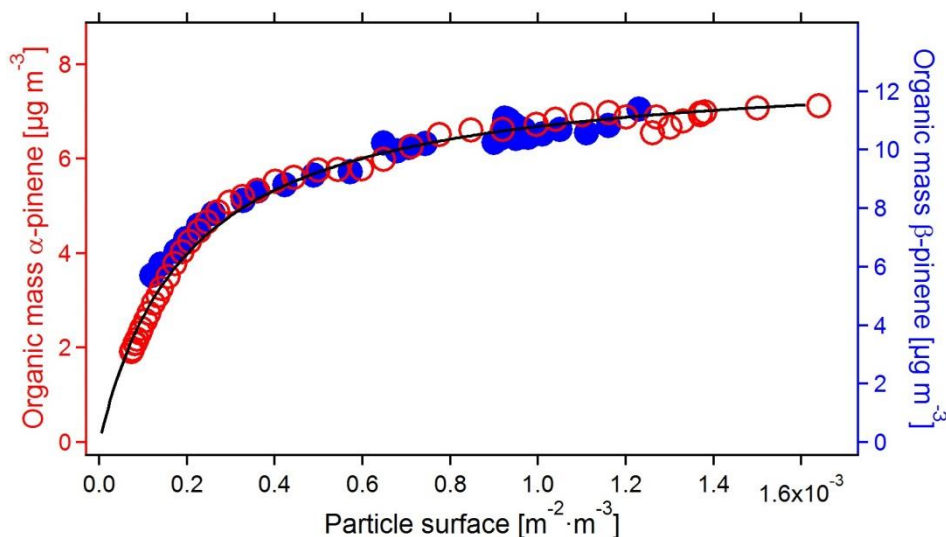
21 Knowing L_W and L_P for a given HOM allows determining the fraction of HOMs that add
 22 mass to particles and the fraction that is lost on the chamber walls. The fraction of the HOMs
 23 contributing to particle mass formation, F_P , is:

$$F_P(H) = \frac{L_P(H)}{L_P(H) + L_W(H)} \quad (\text{ES6})$$

1 As $L_P(H)$ depends on the actual particle surface, $F_P(H)$ also depends on the actual particle
 2 surface. At negligible low particle surface ($L_W \gg L_P$) all HOMs are lost on the walls of our
 3 chamber. At high particle surface ($L_P \gg L_W$) losses of HOMs on the chamber walls are
 4 negligible.

5 During some of the experiments with variations of seed particle surface and at constant
 6 production rates of HOMs, the organic fraction of the particles was determined by Aerosol
 7 Mass Spectrometry, AMS. Thus, the organic mass formed on the seed particles could be
 8 compared to Eq. (ES6) (Fig. S4):

9



10

11 **Figure S4.** Organic mass on seed particles as a function of particle surface in experiments
 12 where production rates of HOMs were held constant and seed particle concentrations were
 13 diminished by stopping seed addition. Open red circles: α -pinene photooxidation, left y-scale.
 14 Closed blue circles: β -pinene photooxidation, right y-scale. While the measurements with α -
 15 pinene were performed at low NO_x conditions ($[\alpha\text{-pinene}]/[\text{NO}_x] \sim 33 \text{ ppbC}\cdot\text{ppb}^{-1}$) the
 16 measurements with β -pinene were performed at high NO_x conditions ($[\beta\text{-pinene}]/[\text{NO}_x] \sim 1.8$
 17 $\text{ppbC}\cdot\text{ppb}^{-1}$). The black line indicates $F_P(H)$ calculated for $\gamma_{eff} = 1$, $\bar{v} = 131 \text{ m s}^{-1}$, i.e. mass
 18 of the HOM = 280 amu, wall loss rate = 0.0067 s^{-1} (lifetime versus wall losses = 150 s,
 19 compare Fig. S2). For better comparability with the measured data points, $F_P(H)$ was
 20 multiplied by 13 ($F_P(H)$ ranges from 0 to 1). Particle surface was varied by varying

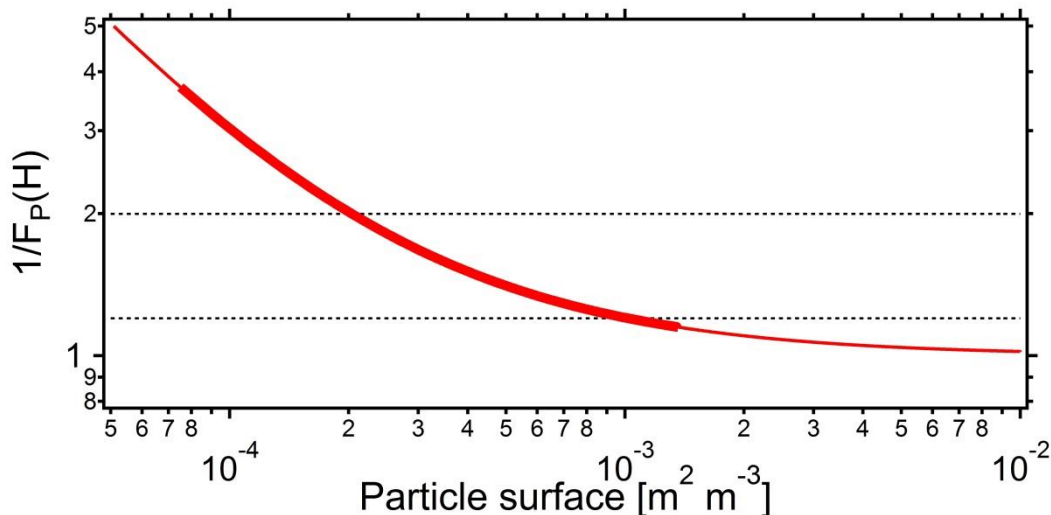
1 concentrations of ammonium sulfate particles (max $\sim 88.5 \mu\text{g m}^{-3}$, mean diameter ~ 70 nm,
2 polydisperse).

3 As already noted by Ehn et al. (2014), wall losses of HOMs generally depended on the mass
4 of the HOM. We assume that the air in our chamber is well mixed except of a boundary layer
5 near to the walls of the chamber. This boundary layer with about 1 mm thickness can be
6 penetrated by molecular diffusion. According to the mass dependence of diffusion
7 coefficients, a heavier HOM (e.g. a dimer = C_{20} oxidation product) diffuses slower through
8 the boundary layer than a lighter HOM. Different diffusion through the boundary layer leads
9 to the different wall losses.

10 As an approximation, ratios of diffusion coefficients for different molecules (diluted in air)
11 depend on the inverse of the square root of the molecules masses. This is because the mean
12 velocity \bar{v} of the molecule also depends on the inverse of the square root of masses. As
13 collisional cross sections of the dominant air molecules (N_2 and O_2) are the same, diffusion
14 coefficients are proportional to \bar{v} . Wall losses of HOMs in our chamber therefore are assumed
15 to be proportional to \bar{v} , even though the precision of HOM measurements did not allow to
16 conclude this for all HOMs.

17 Equation (ES5) which describes $L_p(H)$ also contains \bar{v} . Hence, \bar{v} can be factored out in the
18 denominator of Eq. (ES6) and \bar{v} in the denominator cancels out with \bar{v} in the nominator
19 implicitly enclosed in $L_p(H)$. For simplicity, the fraction of HOMs contributing to particle
20 mass formation is assumed to be independent of \bar{v} and thus independent of the mass of the
21 given HOM. $F_p(H)$ as shown at the example of a certain HOM (Fig. S4, black line) therefore
22 applies to all HOMs with γ_{eff} near to 1.

23 Also semivolatile HOMs can be precursors of mass formation in our chamber. To what
24 amount, is again determined by $F_p(H)$ and thus by γ_{eff} . Assuming that wall losses scale with
25 losses on particles when both surfaces are not reactive, the contribution of semivolatiles to
26 particles also follows $F_p(H)$. Only if one of the surfaces is reactive, semivolatiles may be lost
27 preferentially on the respective surface and their contribution to particle mass might be higher
28 or lower than described by $F_p(H)$. If such processes would be important, a difference between
29 the experimental data and $F_p(H)$ should be visible. For α -pinene and β -pinene as SOA
30 precursors and ammonium sulfate as seed particles no such differences were observed. We
31 therefore suggest that $1/F_p(H)$ can be used to correct measured particle masses. Figure S5
32 shows the values for $1/F_p(H)$ that were used.



1
 2 **Figure S5.** Plot of $1/F_P(H)$ versus particle surface (thin red line). The thick red line shows $1/$
 3 $F_P(H)$ in the range where the measurements with β -pinene were made. The dashed lines are
 4 added to guide the eye. Their crosses with $1/F_P(H)$ show at which particle surface 50 % of the
 5 HOMs are lost on the walls ($1/F_P(H)=2$, $S_p = 2.05 \times 10^{-4} \text{ m}^2 \text{ m}^{-3}$) and when 20 % are lost on
 6 the walls ($1/F_P(H)=1.2$, $S_p = 1.02 \times 10^{-3} \text{ m}^2 \text{ m}^{-3}$) i.e. 80 % contribute to particle formation.

7
 8 Besides wall losses of particle precursors also wall losses of particles itself may skew results
 9 of yield determinations. We found losses of small particles in our chamber. As described by
 10 Wildt et al. (2014) the loss rates of particles with diameters smaller than 7 nm are $0.0017 \pm$
 11 0.0001 s^{-1} , i.e. about 5 times lower than the losses of monomer HOMs. However, when
 12 measuring yields, particle diameters were in the range of $\sim 50 - 150 \text{ nm}$ for which wall losses
 13 are much lower (Mentel et al., 2009) and negligible compared to the losses of HOMs. The
 14 lower wall losses of particles compared to the wall losses of HOMs, are understandable from
 15 a boundary layer at the surface of the chamber walls and the much slower diffusion of
 16 particles compared to the diffusion of HOMs through this layer.

17 As mentioned by Ehn et al. (2014) HOMs contribute the majority of SOA mass at low mass
 18 loadings. Even at SOA mass densities around $10 \mu\text{g m}^{-3}$ they contribute to about two thirds to
 19 the formed SOA mass. As we measured at mass loadings between 10 and $30 \mu\text{g m}^{-3}$, the
 20 contribution of HOMs might be somewhat lower and, as a lower limit we here assume a
 21 contribution of one third. We now estimate the mass loss in our chamber by losses of HOMs,
 22 $[\text{HOM}] \cdot L(\text{HOM})$, in relation to the mass losses of particles, $[\text{P}] \cdot L(\text{P})$:

1
$$\frac{[HOM] \cdot L(HOM)}{[P] \cdot L(P)} \quad (ES7)$$

2

3 Wall loss rates for particles with diameters around 100 nm were $\sim 7.7 \cdot 10^{-5} \text{ s}^{-1}$, loss rates for
4 HOMs were $\sim 0.0067 \text{ s}^{-1}$. With one third of the particles being produced from HOMs,
5 Equation ES7 gives about 26 times faster mass loss in form of HOMs than mass losses in
6 form of particles. At the particle sizes appearing during our measurements on SOA formation,
7 losses of particle precursors were much more important than losses of particles itself.

8

9 As observed from Fig. S4, the organic mass on top of the seed nearly exactly followed the
10 predictions of Eq. (ES6). This implies that $F_p(H)$ is an important property of a chamber,
11 determining mass formation in experiments. If particle surface is known also $F_p(H)$ is known
12 and $1/F_p(H)$ can be used to correct for the losses of HOMs on the walls of the chamber. This
13 allows finding much better numbers for yields than without consideration of wall losses.

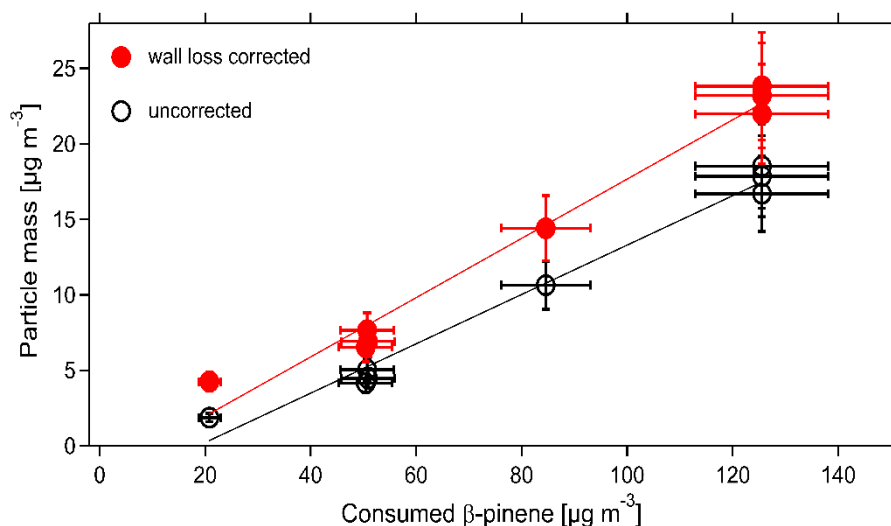
14

15

16 **S2 Determination of yields with consideration of HOM wall losses**

17 Yields of mass formation were determined similar to the procedure described by Mentel et al.
18 (2009). After inducing OH production, particle masses increased, passed a maximum and
19 decreased thereafter. The maximum particle mass measured during experiments with different
20 BVOC concentrations were plotted as a function of consumed α -pinene or β -pinene,
21 respectively. Different to the procedure described by Mentel et al. (2009) we now use masses
22 corrected for wall losses of HOMs. The masses measured at the maxima were multiplied by $1/$
23 $F_p(H)$ that itself was obtained from the measured particle surface using Eq. (S6). As in
24 Mentel et al. (2009) this procedure resulted in linear relationships. The slopes were used to
25 determine the incremental mass yields. Compared to the yields determined without
26 considering wall losses for HOMs, we obtained higher yields. An example is shown in Fig.
27 S6. Data for this example are those of the low OH experiment shown in Fig. 3 of the
28 manuscript.

29



1
 2 **Figure S6.** Produced particle mass as a function of consumed β -pinene. Formally, the yield
 3 for the uncorrected data would be $16 \pm 1 \%$; the yield obtained from the wall loss corrected
 4 masses is: $20 \pm 1 \%$. $1/F_p(H)$ was around 1.3 at high surfaces up to 2.3 at the lowest surface.

5
 6 The differences obtained for the yields with and without wall loss corrections were clear but
 7 in many cases not very high. This is due to the dependence of $1/F_p(H)$ on particle surface and
 8 thus on particle mass. The higher the mass of the organic particles the higher is their surface.
 9 Hence, $1/F_p(H)$ is quite low at high masses whereas it can be high at low masses. The higher
 10 $1/F_p(H)$ at lower masses and lower $1/F_p(H)$ at higher masses dampen the effect of correcting
 11 the particle mass for wall losses.

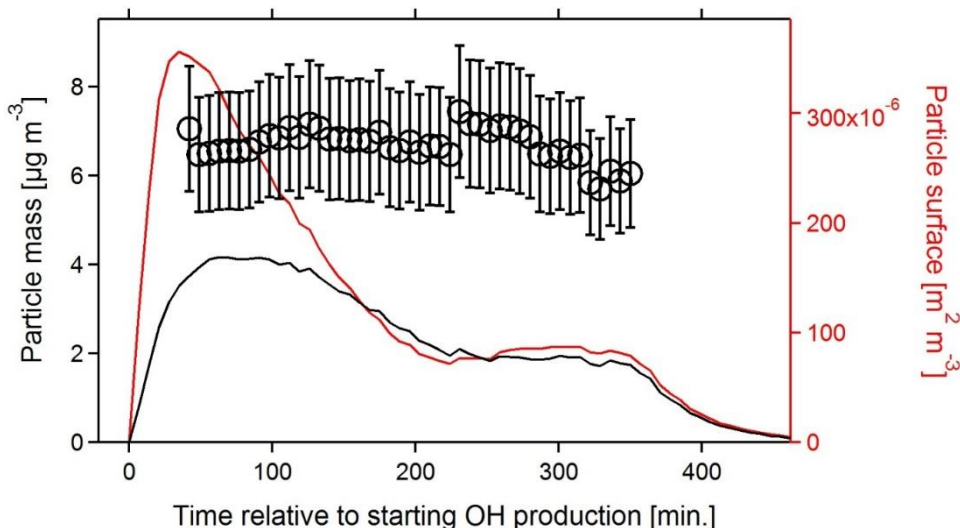
12
 13 **S3 Mass yields obtained from maximum particle masses and steady state particle masses**

14 Using α - or β -pinene concentrations above 0.2 ppb (in the chamber with OH and at steady
 15 state) the particle masses did not decrease to zero after reaching a maximum but stayed on a
 16 certain level. Particle masses at steady state were often substantially lower than at the
 17 maxima.

18 The lower masses were accompanied by lower surfaces. Consequently, $1/F_p(H)$ was higher
 19 during steady state than during the maximum. Correcting the masses measured during the
 20 maxima as well the masses measured during steady state for wall losses of HOMs diminished
 21 these differences to very low amounts.

22 As an example, in an experiment with quite low particle surfaces ($3.6 \times 10^{-4} \text{ m}^2 \text{ m}^{-3}$ in the
 23 maximum, $7 \times 10^{-5} \text{ m}^2 \text{ m}^{-3}$ at steady state; corresponding $1/F_p(H) = 1.57$ at the maximum,

1 3.83 in steady state) Fig. S7 shows the temporal shapes of measured particle mass (= particle
2 volume assuming spherical particles with density 1.2 g cm^{-3}) and the particle mass after
3 correcting the measured particle mass by $1/F_p(H)$ as determined from the measured surface.



4
5 **Figure S7.** Temporal shapes of experimental data and wall loss corrected masses. Black line,
6 left y-axis = measured particle mass assuming spherical particles with a density of 1.2. Black
7 circles, left y-axis = particle mass corrected for wall losses of HOMs. Red line, right y-axis =
8 measured particle surface. OH production was initiated at $t = 0$ minute and stopped at 360
9 minutes. Error bars represent an uncertainty of $\pm 20 \%$ (see error estimate, Sect. S4).

10 While the measured mass decreased by 50 % after reaching the maximum, the masses
11 corrected for wall losses were similar for the time when the measured particle masses were in
12 their maxima and during steady state, respectively.

13 It has to be noted that accounting properly for the dynamics in the wall loss correction was
14 complicated. In particular the data obtained during the first 20 to 30 minutes after initiating
15 OH production were skewed indicating a time shift between particle surface and $1/F_p(H)$.
16 Possibly, it required a certain time until mass had accumulated. For the transient decrease
17 correction factors were taken from the surface measured 21 minutes before. Reason for
18 choosing 21 minutes was the 7 minute time resolution of SMPS measurements and the finding
19 that it took 3 measurement cycles with the SMPS to be near to the maximum mass. Data are
20 only shown for the time period after the maximum particle surface was reached.

21 Such time lags had no impacts on our considerations concerning steady state conditions.
22 Within the error limits, the particle masses obtained during the maximum and during steady
23 state were the same after correcting the data for wall losses. Hence, also the same yields of

1 particle formation were obtained independent of using data from the maxima or during steady
 2 state conditions (compare also data for SOA yields determined by these different methods
 3 given in Table 1 of the manuscript).

4 To calculate the yields during steady state conditions we considered the following processes:
 5 inflow and outflow of particles, losses of particles on the chamber walls, and formation of
 6 particle mass during oxidation of β -pinene with a yield y . Losses of HOMs were neglected
 7 since the particle mass was already corrected for wall losses of HOMs. Expressing the rates of
 8 the processes in- and outflow of particle mass in the continuously stirred tank reactor, wall
 9 loss of particles, and mass formation by oxidation of the precursor leads to the differential Eq.
 10 (ES8):

$$\frac{d[PM]}{dt} = \frac{F}{V} \cdot ([PM]_{in} - [PM]) - [PM] \cdot v^w \cdot \frac{A^w}{V} - y \cdot (k^{OH} \cdot [OH] + k^{O_3} \cdot [O_3]) \cdot [\beta p] \quad (ES8)$$

11 In Eq. (ES8), $[PM]_{in}$ is the particle mass concentration in the inlet airflow and $[PM]$ is the
 12 particle mass concentration in the chamber, respectively. F is the air flow through the
 13 chamber, and V the volume of the chamber. $[PM] \cdot v^w \cdot \frac{A^w}{V}$ represents the wall loss rates of
 14 particles described by the deposition velocity of the particles on the walls, v^w , and the area of
 15 the walls A^w . $(k^{OH} \cdot [OH] + k^{O_3} \cdot [O_3]) \cdot [\beta p]$ describes the oxidation rate of β -pinene. k^{OH}
 16 and k^{O_3} are the rate constants of β -pinene + OH and β -pinene + O₃ reactions, $[OH]$, $[O_3]$, and
 17 $[\beta p]$ are the concentrations of OH, O₃, and β -pinene in the chamber, respectively.

18 At the conditions of our experiments the oxidation rate by OH exceeded that by O₃ by far
 19 allowing neglecting O₃ reactions. $[PM]_{in}$ was near to zero and, for the large particles during
 20 steady state (120-200 nm) wall losses were also negligible. From steady state it then follows:

$$\frac{F}{V} \cdot [PM] = y \cdot k^{OH} \cdot [OH] \cdot [\beta p] \quad (ES9)$$

21 Neglecting ozone reactions also for the calculations of $[OH]$ (see Eq. (2) of the manuscript)
 22 $[OH]$ can be expressed as:

$$[OH] = \frac{F}{V} \cdot \frac{[\beta p]_{in} - [\beta p]}{[\beta p] \cdot k^{OH}} \quad (ES10)$$

1 Exchanging [OH] in Eq. (ES9) by Eq. (ES10) leads to:

$$y = \frac{[PM]}{[\beta p]_{in} - [\beta p]} \quad (ES11)$$

2 which is the very simple assumption of mass transformation from the gas phase to the
3 particulate phase: particle mass is formed from a certain amount of consumed precursor.
4 During steady state conditions, yields were calculated from Eq. (ES10).

5 This procedure allowed adjusting OH concentrations during measurements: Varying $J(O^1D)$
6 caused variations of [OH] and therewith also variations of β -pinene consumption as well as
7 formed particle mass. After variations of $J(O^1D)$, new steady state conditions were reached
8 within 2 -3 exchange times of the air in the chamber. Then the SOA yields were again
9 obtainable from particle masses measured in the new steady state after correcting them for
10 wall losses and the β -pinene consumption.

11 Furthermore, this procedure had advantages for our measurements on NO_x dependencies of
12 SOA formation. During measurements with OH (TUV lamp on, with primary OH
13 production), NO_x concentrations in our chamber were depleted (due to $NO_2 + OH (+M) \rightarrow$
14 $HNO_3 (+M)$ reactions) but eventually reached a steady state. Yield data from steady state
15 conditions were directly comparable to steady state $[NO_x]_{ss}$. This allowed avoiding usage of
16 $[NO_x]_0$ which might not reflect the chemical behaviour during development of the chemical
17 system. However, using either $[NO_x]_0$ or $[NO_x]_{ss}$ for determinations of NO_x dependencies of
18 yields did not change the behaviour qualitatively (see Fig. 2 in the manuscript). Only the scale
19 of $[NO_x]$ changed since $[NO_x]_0$ was different from $[NO_x]_{ss}$.

20

21 **S4 Uncertainties of the wall loss correction procedure and description of estimated total** 22 **errors**

23 The uncertainty of the correction procedure was estimated as follows: We assumed that the
24 deviation between the measured organic mass and $1/F_p(H)$ was low in the range of particle
25 surfaces covered by the example shown in Fig. S4 (β -pinene: $\sim 1.2 \times 10^{-4} - 1.3 \times 10^{-3}$, α -
26 pinene $\sim 1 \times 10^{-4} - 1.6 \times 10^{-3} \text{ m}^2 \text{ m}^{-3}$). The error caused by our correction procedure should
27 approach zero for $1/F_p(H) \sim 1$ i.e. $L_p \gg L_w$. The error furthermore should increase with
28 higher $1/F_p(H)$. We arbitrarily set the maximum deviation between the theoretical function of
29 $F_p(H)$ and the measured data to 10 % in the range where the measurements were made (see

1 Fig. S4). Considering that the error is zero at $1/F_p(H) = 1$, the uncertainty of wall loss
2 corrections can be set to $(1/F_p(H)-1) \times 0.1$ in the respective range. This is considered as the
3 relative error caused by applying the correction for wall losses. Multiplying $(1/F_p(H)-1) \times 0.1$
4 with the measured particle mass (data from the black line in Fig. S6) gives the absolute
5 uncertainty for the extrapolated data (error bars at circles in Fig. S6). Please note that this is
6 only the error from the wall loss correction procedure, errors in the experimental
7 determination of particle masses and particle surfaces are not included here.

8 $F_p(H)$ strongly decreases with lower particle mass/surface. It is therefore obvious that the
9 possible error in determination of wall loss corrected particle masses becomes the higher the
10 lower the measured particle surface is. This is included in the error estimation as it includes
11 $1/F_p(H)$. We nevertheless used higher relative errors for lower particle surfaces by setting
12 them arbitrarily to 20 % for $2 < 1/F_p(H) < 5$, to 30 % for $5 < 1/F_p(H) < 10$, and to 40 % and
13 for $10 < 1/F_p(H)$.

14 It has to be noted that for our α -pinene experiments where low concentrations were used,
15 particle surfaces were quite low in particular when new particle formation was suppressed due
16 to high NO_x concentrations (see also Wildt et al., 2014). In case of such low surfaces $1/F_p(H)$
17 exceeded 10. SOA yields derived at high NO_x levels therefore may have very high
18 uncertainties. However, neglecting wall losses the effects of NO_x would be strongly
19 overestimated.

20 With particle surface increasing above $1 \times 10^{-3} \text{ m}^2 \text{ m}^{-3}$ $F_p(H)$ only slightly increases and
21 approaches unity. Errors of mass determination due to neglecting wall losses for HOMs
22 therefore become negligible. However, at higher particle surfaces there may be other
23 processes besides those considered here. As an example: if the lifetime of a volatile
24 compound versus wall losses exceeds the residence time of our chamber, a large fraction of
25 this compound will be flushed out. For such a compound F_p cannot be defined in the way as
26 given by Eq. (ES6). If such semi-volatile compounds would be taken up by particles due to
27 another process than physical condensation, organic mass on particles can increase stronger
28 than extrapolated from Fig. S4. As our measurements were restricted to particle surfaces
29 below $1.6 \times 10^{-3} \text{ m}^2 \text{ m}^{-3}$ the previous considerations on wall loss corrections are only valid up
30 to this limit (particle surface $1.6 \times 10^{-3} \text{ m}^2 \text{ m}^{-3}$, equivalent to particle mass $88.5 \mu\text{g}$ for our
31 polydisperse ammonium sulfate seed particles with a mean diameter of 70 nm). Furthermore,
32 these considerations are only valid for α -pinene and β -pinene and for concentrations below 10
33 ppb (during OH oxidation in the chamber). Oxidation products of other volatiles may show

1 behaviour different from that shown in Fig. S4. Similarly, very high VOC concentrations
2 might also cause deviations from the behaviour shown here.

3 Besides possible errors from our wall loss correction procedure there are also possible
4 systematic errors caused by calibration errors of the analytic devices. In particular BVOC
5 concentrations and thus BVOC consumptions, NO_x concentrations, and particle mass
6 densities are possible error sources. We estimate the respective systematic errors to ± 10 %
7 for BVOC-, NO_x-, particle mass- and particle number data. Such errors certainly affect the
8 precision of yield data. However, for determinations of NO_x dependencies, systematic errors
9 in BVOC concentration data and particle mass data are less important. Comparing yields
10 obtained in an experiment series where the same BVOC device and the same SMPS were
11 used is a comparison of relative data. In yield plots, we show the sum of the systematic error
12 and the error caused by our correction procedure.

13 Error limits for the yields are calculated from error propagation using the sum of systematic
14 error and error from the correction procedure and 10 % for BVOC data. In case of yields
15 plotted versus NO_x, we show 10 % error for NO_x data (Figs. 2, 5, 7, 8, and 10). Plotting [OH]
16 versus NO_x we give 20 % error for [OH] (see manuscript) and 10 % error for [NO_x],
17 respectively (Figs. 4 and 6). For the plot of mass data versus BVOC consumption (Fig. 3) we
18 show the error limits as estimated for particle mass, i.e. sum of 10 % systematic error and
19 error from the correction method and 10 % for the BVOC consumption. The error limits given
20 in the text for the yields given in Fig. 3 represent the statistical error from the plot only. For
21 the plot of particle number versus NO_x (Fig. 9) we give 10 % error for particle number and
22 NO_x data.

23 Considering that the ratio [BVOC]₀/[NO_x]₀ contains possible errors in both quantities, the
24 error for [BVOC]₀/[NO_x]₀ was calculated according to error propagation (Fig. 1).

25

26

27 **References to supplemental information**

28 Ehn, M., Thornton, J. A., Kleist, E., Sipilä, M., Junninen, H., Pullinen, I., Springer, M.,
29 Rubach, F., Tillmann, R., Lee, B., Lopez-Hilfiker, F., Andres, S., Acir, I.-H., Rissanen, M.,
30 Jokinen, T., Schobesberger, S., Kangasluoma, J., Kontkanen, J., Nieminen, T., Kurtén, T.,
31 Nielsen, L. B., Jørgensen, S., Kjaergaard, H. G., Canagaratna, M., Dal Maso, M., Berndt, T.,
32 Petäjä, T., Wahner, A., Kerminen, V.-M., Kulmala, M., Worsnop, D., Wildt, J., and Mentel,
33 T. F.: A large source of low-volatility secondary organic aerosol. *Nature*, 505, 476-479, 2014.

1 Mentel, Th. F., Wildt, J., Kiendler-Scharr, A., Kleist, E., Tillmann, R., Dal Maso, M., Fisseha,
2 R., Hohaus, Th., Spahn, H., Uerlings, R., Wegener, R., Griffiths, P., Dinar, E., Rudich, Y.,
3 and Wahner, A. (2009) Photochemical production of aerosols from real plant emissions.
4 *Atmos. Chem. Phys.*, 9, 4387-4406, 2009.

5 Mentel, T. F., Springer, M., Ehn, M., Kleist, E., Pullinen, I., Kurtén, T., Rissanen, M.,
6 Wahner, A., and Wildt, J.: Formation of highly oxidized multifunctional compounds:
7 autoxidation of peroxy radicals formed in the ozonolysis of alkenes – deduced from structure–
8 product relationships, *Atmos. Chem. Phys.*, 15, 6745-6765, 2015.

9 Wildt, J., Mentel, T. F., Kiendler-Scharr, A., Hoffmann, T., Andres, S., Ehn, M., Kleist, E.,
10 Müsgen, P., Rohrer, F., Rudich, Y., Springer, M., Tillmann, R., and Wahner, A.: Suppression
11 of new particle formation from monoterpene oxidation by NO_x . *Atmos. Chem. Phys.*, 14,
12 2789–2804, 2014. doi:10.5194/acp-14-2789-2014.